energies

MDPI

Article

Prevention of Wildfires Using an AI-Based Open Conductor Fault Detection Method on Overhead Line

Junsoo Che, Taehun Kim, Suhan Pyo, Jaedeok Park, Byeonghyeon An and Taesik Park *

Department of Electrical and Control Engineering, Mokpo National University, Muan 58554, Republic of Korea
* Correspondence: tspark@mokpo.ac.kr

Abstract: Overhead lines that are exposed to the outdoors are susceptible to faults such as open conductors on weak points and disconnection caused by external factors such as typhoons. Arcs that occur during disconnection generate energy at a high heat of over 10,000 °C, requiring swift fault shut-off. However, most conventional fault detection methods to protect electrical power systems detect an overcurrent; thus, they can only detect faults after the line is disconnected and the cross-section of the line that generates the arc discharge makes contact with another line or the ground, causing a high risk of fire. Furthermore, in the case of ground faults owing to the disconnection of overhead lines, the load and the grounding impedance are not parallel. Therefore, in the case of the fault current not exceeding the threshold or a high impedance fault due to the high grounding impedance of the surrounding environment, such as grass or trees, it is difficult to determine overhead line faults with conventional fault detection methods. To solve these issues, this paper proposes an AI-based open conductor fault detection method on overhead lines that can clear the fault before the falling open conductor line comes into contact with the ground's surface so as to prevent fire. The falling time according to the height and span of the overhead line was calculated using a falling conductor model for the overhead line, to which the pendulum motion was applied. The optimal input data cycle that enables fault detection before a line–ground fault occurs was derived. For artificial intelligence learning to prevent wildfires, the voltage and current signals were collected through a total of 432 fault simulations and were wavelet-transformed with a deep neural network to verify the method. The proposed total scheme was simulated and verified with MATLAB.

Keywords: open conductor fault; deep neural network; fire protection; fault detection; high impedance fault

Citation: Che, J.; Kim, T.; Pyo, S.; Park, J.; An, B.; Park, T. Prevention of Wildfires Using an AI-Based Open Conductor Fault Detection Method on Overhead Line. *Energies* **2023**, *16*, 2366. https://doi.org/10.3390/en16052366

Academic Editor: Silvio Simani

Received: 9 January 2023
Revised: 6 February 2023
Accepted: 15 February 2023
Published: 1 March 2023

1. Introduction

Faults in electrical power systems can cause financial loss and casualties; thus, the development of fault detection methods for electrical power systems is a key research area for many researchers [1–3]. Since 1901, when the first electro-mechanical induction relay emerged to protect electrical power systems, electrical power system protection methods have continuously developed, including ultrahigh speed, adaptive protection, AI-based protection, and others [4]. Despite such efforts, however, there is still a risk of fire owing to faults in overhead lines [5]. If a fault detection system cannot detect line faults in time, arcs with high heat are generated at the point of the fault and can cause combustion, leading to wildfire [6]. According to [7], many fires in recent years have been caused by downed power lines used by The California Public Utilities Commission, and at least 17 out of 21 major fires in Northern California in the Fall of 2018 were determined to have occurred due to electrical lines and utility poles. Fires caused by line faults, in turn, affect power grids, resulting in problems in the operation of electrical power systems [8]. Thus, faults in electrical power systems need to be removed as quickly as possible. While there are various scenarios where overhead line faults can occur, this study considered a specific scenario where an overhead line breaks and falls on the ground. Conventional high-impedance

fault (HIF) and downed powerline detection methods can detect faults once the line comes into contact with the ground [5,9–16]. In this case, even if a fault detection process takes action and clears the fault, the arc at the cross-section of the line generates high heat, over 10,000 °C, resulting in a risk of fire in a short space of time. Therefore, areas where overhead lines run through mountains or forests, particularly areas that are dry with many deciduous leaves, require additional means for preventing wildfire.

Therefore, various studies have been conducted to deal with faults, including open conductor faults, which are also called broken conductor faults. The authors of [17] proposed a time-shifting method for determining open conductor faults in distribution systems' overhead lines. While the difference in the voltage vector that changes in the case of faults was verified by simulation, a concrete application plan using the changed voltage vector could not be presented. The authors of [18] proposed a sequence component method that determined open conductor faults by using the ratio of the positive sequence component current and the negative sequence component current. However, this method cannot be used in situations where there is an unbalanced load. The authors of [19] proposed installing an open conductor detector between loads and lines, considering that the voltage would drop when measuring the power supply due to the high load of open conductors and subsequent HIF faults. While this method is simple and can be a good solution, it is inefficient in terms of cost due to the number of detectors needed in those areas. EPRI proposed two open conductor detection methods [20,21]. One involves determining the open conductor status by measuring the excitation current after applying the voltage source to the neutral point of the transformer. This determines whether it is an open conductor if the current is low. The disadvantage is that a large amount of money needs to be invested in a new, additional voltage source. The second method involves determining faults by monitoring the 1, 3, 5, and other harmonic components of the neutral current and checking the changes in the frequency content. Open conductor faults cause a rapid change in the frequency content, and the arcs generated by such faults produce current waves with a high-frequency content and a voltage imbalance. In addition, HIF caused by an open line making contact with the ground's surface generates a fault current at a high frequency due to the arc [22–24]. This method is more efficient than the first in terms of cost.

However, it is difficult to determine an open conductor by setting a frequency threshold value. The measured frequency content can be affected by other factors, including the power conversion system (PCS) used when the distributed resources are connected, power capacitors for compensating reactive power, the exciting current of the transformer, corona, and harmonic content from loads [25–27]. Thus, a new open conductor detection method is required that uses frequency as an input but does not use a threshold. The authors of [28,29] recognized this issue. The authors of [28] proposed a method that detects open conductors using the third harmonic content, and the authors of [29] determined open conductors by verifying the zero-sequence voltage at the neutral point, current imbalance, and changes in the current frequency. Since the zero-sequence current at each phase flows to the neutral point, this can determine open conductors to measure the zero-sequence voltage and current at the neutral point. However, the authors of [28,29] could not detect the open conductor location or type. Since an artificial neural network can classify minute differences in the data that cannot be differentiated by the human eye through learning the patterns of the class that need to be differentiated, it has been used in open conductor fault detection [30,31]. However, the authors of [30,31] did not use a feature extraction process, and thus high accuracy cannot be expected. In addition, the measuring points were located at the ends of the protection line, which requires measuring devices on both ends of the region that need to be protected. Since the phase of input data is not considered, a high-speed fault diagnosis is difficult because the point at which fault detection is possible resets every cycle. The research topic of diagnosing transmission line faults using a deep neural network (DNN) with wavelet transform has been widely studied [32–37]. The authors of [32] studied the extraction of features via wavelet transformation and the

diagnosis of line faults using naive Bayes. Input data were measured with a sampling frequency of 20 kHz and 333 data points per cycle. However, the authors of [32] did not consider the cycle of the measuring equipment installed in the actual system. Therefore, this method cannot be used without STATCOM. The authors of [34] diagnosed line faults using wavelet transform and a convolutional neural network (CNN). The authors of [35–38] also extracted feature quantities using wavelet transform and diagnosed line failures using AI algorithms. However, the authors of [32–37] had no limit on the time taken for fault diagnosis. In addition, these studies were conducted with L2G (line-to-ground fault) and L2L (line-to-line) faults as classification classes, but open conductor faults were not considered. Therefore, this paper proposes a method that diagnoses and clears open conductor faults before said open conductor lines make contact with the surface. Furthermore, the proposed method extracted the features via a wavelet transformation by using the fact that frequency content would change in the case of open conductor faults and performed the training of an artificial neural network model with the wavelet-transformed voltage and current. By comparing the time and accuracy of the input data, the study derived the final model.

2. Problems of Open Conductor Fault

There can be three overall situations that can continue after an open conductor fault.

1. The open conductor fault continues while the disconnected overhead line does not contact the surface or other nearby lines.
2. The open overhead line contacts the surface and overcurrent flows.
3. The open overhead line contacts the surface or other nearby lines, but the fault current is relatively low.

In the first scenario, the open overhead line does not contact the nearby lines, which can happen when the jumper line is broken. A jumper line is installed along with insulators to insulate overhead lines and supporting structures such as steel towers. Since the length of the jumper line is short, it is more likely that it will not contact the steel tower or the surface in the case of its breaking, which leads to the situation where there is no overcurrent [38]. The second scenario is the fault that can be detected by conventional methods owing to a sufficient overcurrent. In the final scenario, the overhead line comes into contact with the surface or nearby lines, but the fault current is relatively low. Such a fault is called HIF, which often occurs when the open line contacts the surface, boughs, or twigs. In this paper, an open conductor fault detection method was proposed to operate a circuit breaker using not the ground fault signal but the open conductor signal when an overhead line is broken and falls to the ground. The conventional impedance-based detection methods can cause the following problems:

- Under-reach, over-reach.
- Undetectable fault.
- Fire due to arcs.

Impedance-based detection methods determine the location of the fault via the ratio of the fault current to the fault voltage in the case of a fault. Assuming that the ground resistance is the same, the line impedance is the only factor, and thus a fault can be determined using the principle that the fault current decreases as much as the length of the line. However, ground resistance can be affected by the weather or season and cannot be the same all the time. In addition, it may differ by the properties of the ground, which may result in under-reach or over-reach that misjudges the fault region. Due to such issues, distance relays are currently used in overlaps to monitor faults [39].

In addition, the HIF that occurs in the case of high ground impedance is problematic. Generally, the fault current is three to six times higher than the rated current, but if the ground impedance is huge, the fault current becomes lower than can be detected as a fault, resulting in a failure to detect the fault. This is often caused by the open overhead line making contact with the ground. If a line-to-ground fault occurs without a broken line, the parallel connection between the ground impedance and the load impedance results in

relatively low impedance and a large fault current, which can be sufficient for detecting a fault. However, if overhead lines are disconnected and make contact with the ground, only the ground impedance exists, causing more frequent HIFs [5,10–14].

The final problem is fire caused by arcs. In the case of open conductor lines, arc discharge occurs due to the potential difference between the conductor and air. At this moment, the arc temperature soars over 10,000 °C, which is very dangerous even for a short amount of time. Arcs can affect inflammable materials with a low flashing point, such as surrounding trees or deciduous leaves, leading to fire [5–7].

3. Proposed Scheme for the Prevention of Wildfire

As a solution to the problems in the conventional methods discussed above, such as fire owing to arcs, this study proposes an AI-based open conductor fault detection method that can perform the circuit breaking operation before the open conductor line contacts the ground.

At the moment of the breaking, the fault current is small, and a relatively low circuit breaking performance is required, and if the measurement is made at the right time, the capacity of the required circuit breaker is small so that the difficulty level of the circuit breaking performance is even lower.

3.1. Falling Conductor Model

Figure 1 is a flowchart of the proposed method. Since the proposed method requires time-series data, common measuring devices such as current transformers (CTs) and potential transformers (PTs) cannot be used. Additionally, the time data of the signal are required, and thus we must collect input data using a PMU. The measured time-series data of the three-phase voltage and current signals are wavelet-transformed. Existing studies for diagnosing line-to-ground and line-to-line faults used the maximum, average, and variance values from the transformed data as inputs. However, since the fault current converges to 0 in an open conductor fault, learning results are poor when a representative feature value such as a maximum is used. Therefore, the wavelet-transformed signals are flattened and input to the fault diagnosis algorithm. The AI-based algorithm diagnosis the open conductor fault and sends a cut-off signal to the circuit breaker. The circuit breaker receives the blocking signal and performs a blocking operation. In the flowchart of Figure 1, the time required from start to end must be strictly observed because the fault blocking must be completed before the line is disconnected and contacts the ground.

The above problems result in the need for a high-speed open conductor fault detection method that is not affected by ground impedance. To develop an algorithm that completes the circuit break process before the broken lines contact the ground, the calculation of the speed at which lines fall to the ground and open conductor signal analysis should be conducted. To remove faulty zones, a protective relay should detect a fault and a circuit breaker should isolate the fault area in the system. The total fault removal time consists of the relay time (fault detection), the circuit breaking time, and the communication time [40]. Thus, the total duration of this whole process and the falling time should be compared.

Figure 2 is an overhead line fault location overview. The length between the towers is the span, and the height is the length between the ground and the line. As is shown in Figure 2, factors that can affect the time of line falling include the span, height, and sag of the line [41]. The falling times that occurred at the fault points A, B, and C in Figure 2 correspond to the values provided in Table 1. Various standards are used in the cables for overhead lines from the distribution to the transmission lines. According to such standards, the weights of lines differ, and the height of the transmission towers and the ground clearance of the transmission lines also differ by voltage level, country, and region. In the USA, generally, NESC 232D [42] is used to determine the ground clearance of lines, but in California where there are many mountains, the height and ground clearance of lines are more strictly regulated than in other states. As such, the time of line falling differs by

such factors that it is necessary to designate the environment and line to which this method is applied.

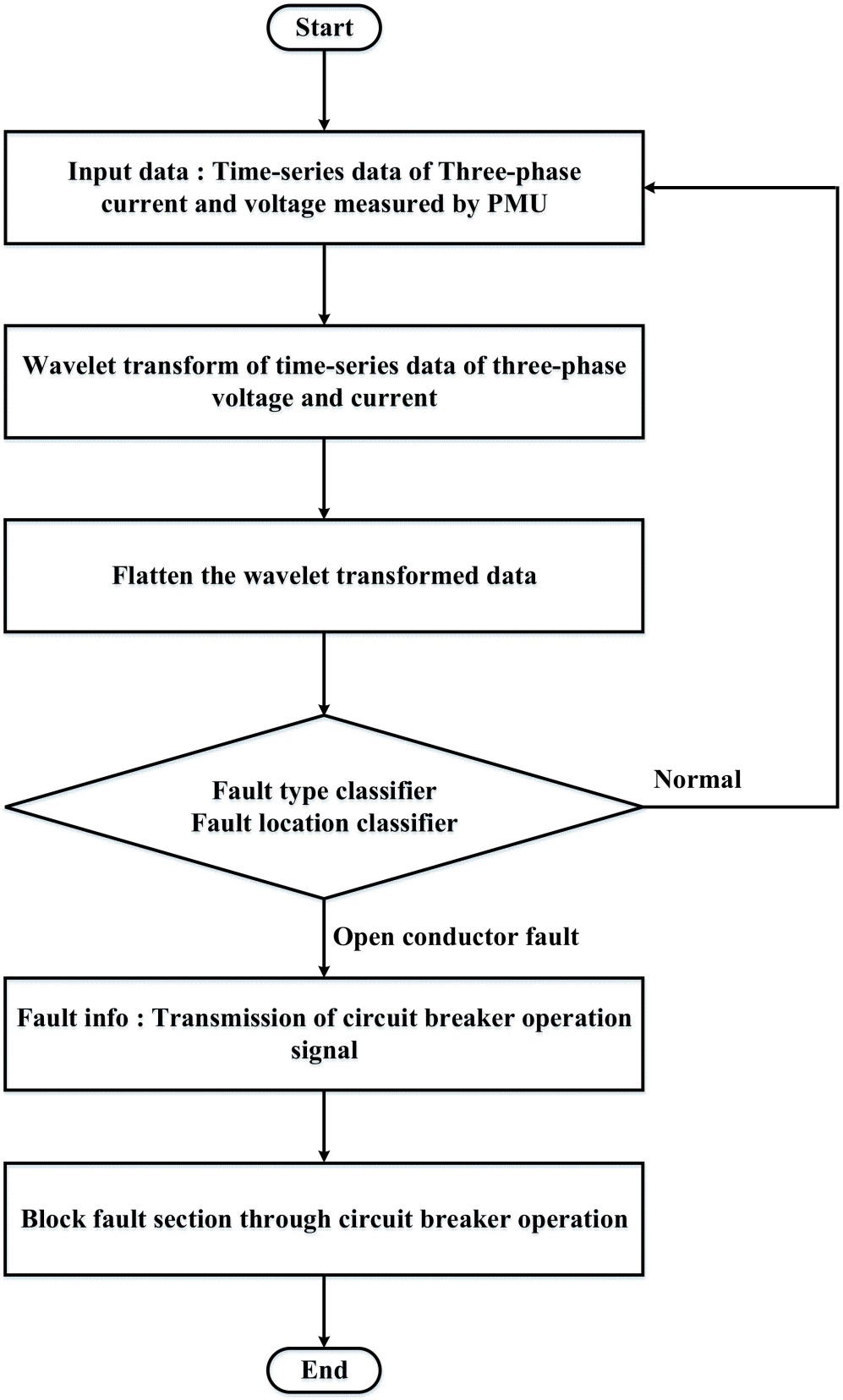

Figure 1. Flowchart of the proposed method.

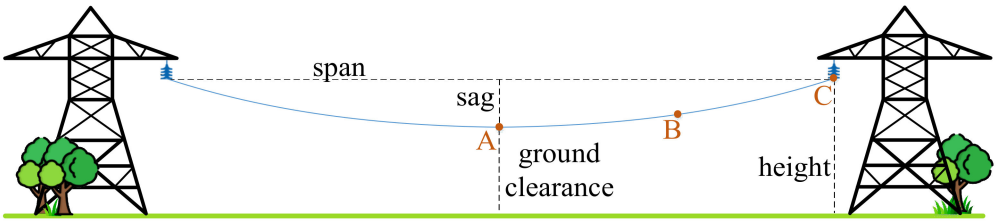

Figure 2. Overhead line fault location overview.

Table 1. Transmission line falling time.

Voltage Level (kV)	Height (m)	Span (m)	Ground Clearance (m) <Tree Type>	Wire Type (mm^2)	Falling Time (s) <A>	Falling Time (s) <B>	Falling Time (s) <C>
154	35	400	21 <Pitch Pine> 24 <Karamatsu> 19 <Other trees>	ACSR 330	0.3504 0.3970 0.3192	0.2813, 0.5278 0.3203, 0.5933 0.2557, 0.4830	0.2425 0.2751 0.2198
345	50	450	24 <Pitch Pine> 26 <Karamatsu> 22 <Other trees>	ACSR 480	0.3888 0.4195 0.3585	0.3081, 0.6120 0.3334, 0.6560 0.2841, 0.5664	0.2639 0.2856 0.2429
765	100	550	28 <Pitch Pine> 31 <Karamatsu> 27 <Other trees>	ACSR 480	0.4566 0.5013 0.4408	0.3476, 0.8427 0.3822, 0.9228 0.3344, 0.8162	0.2917 0.3214 0.2810

This study considered the time of line falling in the case of transmission in mountainous regions in South Korea. The calculation of the timing of the falling of transmission lines that pass through mountainous regions in South Korea is shown in Table 1. South Korea is an urban country where most of the population is concentrated in the capital area, and most energy produced in each region is sent to Seoul. As 65% of the national land is mountainous, most transmission lines run over trees. In addition, even when lines run over mountains or trees, those trees are not removed; therefore, the ground clearance differs by the type of tree over which those lines pass. The height is determined by the voltage level and region, and additional height is added to it according to the type of tree so as to determine the ground clearance based on the final design height. In the case of Pitch Pine, 17.9 m is added, 20.6 m is added for Karamatsu, and 16.2 m is added for other trees.

If transmission towers are managed by a private company, those towers are installed based on economic efficiency, but in South Korea, one public company manages all transmission towers; thus, the ground clearance of transmission towers is set high based on the consideration of various factors, such as strict electric standards, topographic characteristics due to the many mountains, preparation for future power demands, and others, rather than economic concerns. The height of 345 kV transmission towers in South Korea is between 50 and 100 m, and that of 765 kV towers is approximately 90–120 m.

The span between towers can change due to various conditions, such as the altitude difference in the mountains. This study set the span by referring to the Design Standard of Tower for Overhead Transmission Line (DS-1111) in KEPCO. The transmission voltage levels in South Korea are 154, 345, and 765 kV, and the spans are 400, 450, and 550 m (500 m per line), respectively.

The wire type is ACSR (aluminum conductor steel-reinforced), which is mainly used for power transmission, and it is assumed that 500 and 765 kV use multiple conductors and multiple line transmissions.

The fall of transmission lines exhibits an equation of motion similar to that of a pendulum since one end of the line is connected to a tower. In this study, the falling time was calculated by assuming that the falling transmission line is that of a pendulum with its initial speed at 0 [43,44].

The time of falling in Table 1 was calculated from three spots, A, B, and C in Figure 2, as the location at which the break occurred. The shortest falling time was 0.2198 s; thus, the fault detection, communication, and circuit break operation should be completed within this duration.

The falling of overhead lines is more likely to be the result of external factors such as birds, trees, or typhoons than the degradation of lines. Such factors can affect the line falling time. However, this paper disregarded such environmental factors and line elasticity when calculating the falling time.

3.2. Analysis of Open Conductor Fault

To verify the need for open conductor fault detection and develop open conductor fault detection technology, it is necessary to analyze the characteristics unique to open conduction faults, such as the voltage and current signals that change in the case of an open conduct fault [39]. Similar to the verification of the voltage and current changes via the change in impedance through the solution of a differential equation of a circuit, the voltage and current in the case of an open conductor fault can be calculated via the pre-fault voltage and impedance (Zbus) matrices in the electrical power system [41].

$$I_f'' = \frac{V_f}{Z_{kk}} \tag{1}$$

Shown above is the equation of sub-transient current I_f'' in the case of a fault in a bus based on the pre-fault voltage V_f and Thévenin's impedance Z_{kk}, the diagonal element of Zbus. I_f'' is distributed to the whole system in the reference node before it flows from the fault point. In this process, the voltage of the whole bus system changes.

$$V_j = V_f - Z_{jk} I_f'' = V_f - \frac{Z_{jk}}{Z_{kk}} V_f \tag{2}$$

The principle of superposition is added to the voltage before the fault.

$$I_{ij}'' = \frac{V_i - V_j}{Z_b} = -I_f'' \left(\frac{Z_{ik} - Z_{jk}}{Z_b} \right) = -\frac{V_f}{Z_b} \left(\frac{Z_{ik} - Z_{jk}}{Z_{kk}} \right) \tag{3}$$

In the case of an imbalance fault, such as an open conductor in phase A, it can be calculated by using the sequence network based on the symmetrical components proposed by C. L. Fortescue [45]. For an open conductor in phase A, $I_a = 0$, and thus the following equation can be derived:

$$I_a^{(0)} + I_a^{(1)} + I_a^{(2)} = 0 \tag{4}$$

Since phases B and C are not in the open conductor status, the voltage drops are:

$$V_{pp',b} = 0, \;\; V_{pp',c} = 0 \tag{5}$$

$$\begin{bmatrix} V_a^{(0)} \\ V_a^{(1)} \\ V_a^{(2)} \end{bmatrix} = \frac{1}{3} \begin{bmatrix} 1 & 1 & 1 \\ 1 & a & a^2 \\ 1 & a^2 & a \end{bmatrix} \begin{bmatrix} V_{pp',a} \\ 0 \\ 0 \end{bmatrix} = \frac{1}{3} \begin{bmatrix} V_{pp',a} \\ V_{pp',a} \\ V_{pp',a} \end{bmatrix} \tag{6}$$

$$V_a^{(0)} + V_a^{(1)} + V_a^{(2)} = \frac{V_{pp',a}}{3} \tag{7}$$

The open conductor in the phase A results in the same voltage drop results in each sequence network. As the voltage drop in the symmetrical components is identical, and the incoming and outgoing current at the fourth point in the equation are the same, like Kirchhoff's circuit laws, the sum of each current is 0, and the sequence networks can be linked in parallel. Thus, current $I_a^{(1)}$ is:

$$I_a^{(1)} = I_{mn} \frac{Z_{pp'}^{(1)}}{Z_{pp'}^{(1)} + \frac{Z_{pp'}^{(2)} Z_{pp'}^{(0)}}{Z_{pp'}^{(2)} + Z_{pp'}^{(0)}}} = I_{mn} \frac{Z_{pp'}^{(1)} \left(Z_{pp'}^{(2)} + Z_{pp'}^{(0)} \right)}{Z_{pp'}^{(0)} Z_{pp'}^{(1)} + Z_{pp'}^{(1)} Z_{pp'}^{(2)} + Z_{pp'}^{(2)} Z_{pp'}^{(0)}} \tag{8}$$

The voltage drops of symmetrical components $V_a^{(0)}$, $V_a^{(1)}$, and $V_a^{(2)}$ are:

$$V_a^{(0)} = V_a^{(1)} = V_a^{(2)} = I_a^{(1)} \frac{Z_{pp'}^{(2)} Z_{pp'}^{(0)}}{Z_{pp'}^{(2)} + Z_{pp'}^{(0)}} = I_{mn} \frac{Z_{pp'}^{(0)} Z_{pp'}^{(1)} Z_{pp'}^{(2)}}{Z_{pp'}^{(0)} Z_{pp'}^{(1)} + Z_{pp'}^{(1)} Z_{pp'}^{(2)} + Z_{pp'}^{(2)} Z_{pp'}^{(0)}} \quad (9)$$

The value on the right side of the above equation is determined by the impedance parameter of the sequence networks and the pre-fault current in phase A. The above symmetric components are converted into a, b, and c phases, and the voltage and current are calculated. The size of the impedance at the measuring instrument location at the time of open fault is determined by the change in current caused by the load drop. If the dropped load is small, it may be difficult to detect. In addition, since different results are obtained in a system in which distributed power sources are scattered, it can be said that methods for detecting open conductor faults through threshold values are less versatile.

3.3. Proposed Fault Detection Scheme

Figure 3 is an overview of the proposed method. The voltage and current time-series data of the overhead line are collected through the PMU, and these signals are wavelet-transformed to extract features and input to the AI-based open conductor classifier to detect faults.

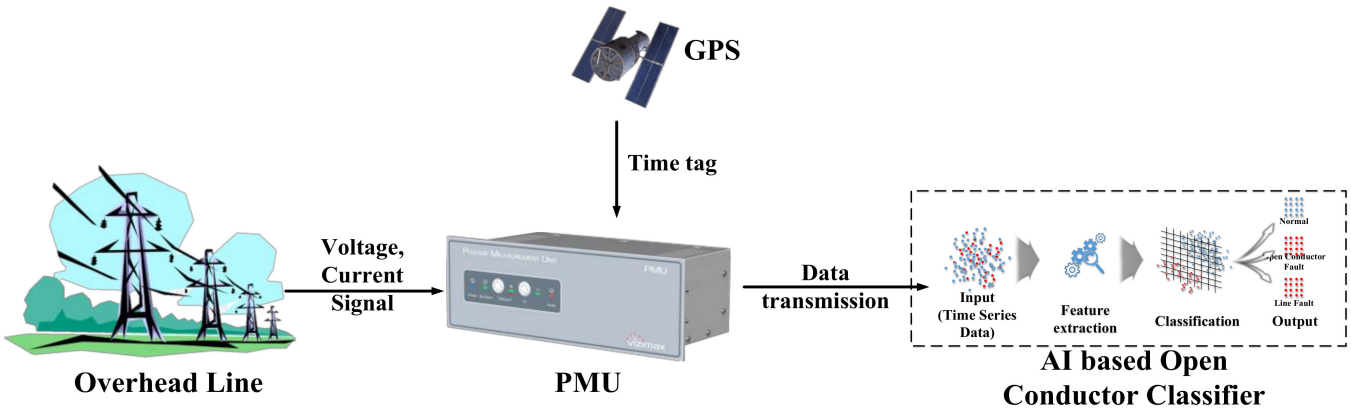

Figure 3. Conceptual diagram of the proposed method.

3.3.1. Deep Neural Network

An artificial neural network is a machine learning model that simulates the information processing of neurons based on the operation principle of the network of nerve cells in the brain. In the past, it was considered impossible to create a meaningful neural network, but with the development of activation functions, such as a restricted Boltzmann machine (RBM), rectified linear unit (ReLU), or GPUs that allow for parallel arithmetic, various studies involving deep learning are now being conducted.

$$f\left(b + \sum_{i=1}^{n} x_i w_i\right) \quad (10)$$

b = bias
x = input to neuron
w = weights
n = the number of inputs from the incoming layer

Figure 4 shows the training process of the proposed method. The three-phase time-series voltage–current signal is used as the input of the deep neural network (DNN) after wavelet transformation and flattening. An artificial neural network consists of the input, hidden, and output layers, and a DNN has two or more hidden layers. Having received

the input data, neurons produce outputs and send them to the next neuron, and this input and output process of the neurons can be expressed using Equation (10).

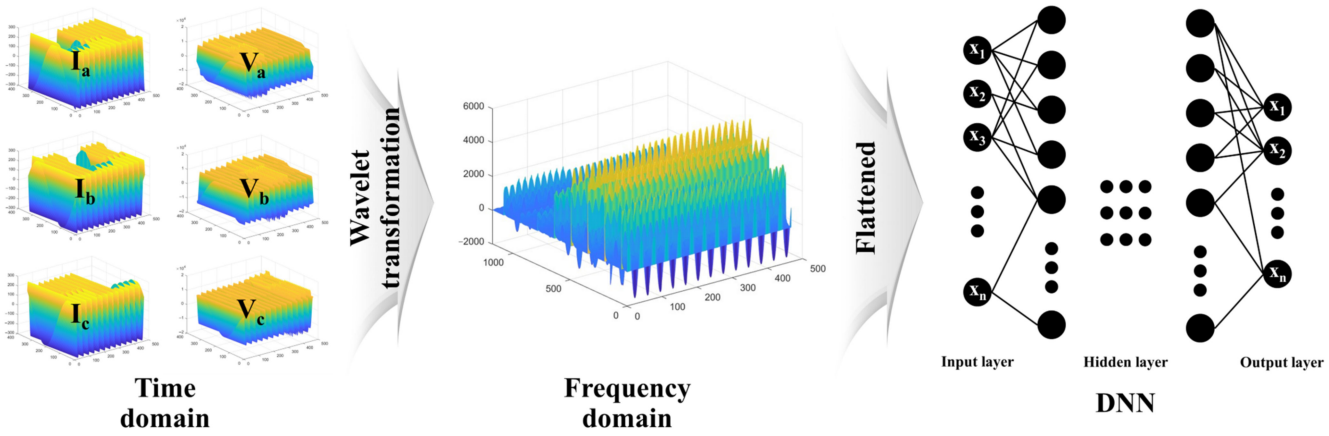

Figure 4. DNN training process of the proposed method.

The activation function, f, in Equation (10) converts the output value so that it is suitable for the artificial neural network and usually uses the ReLU function, which helps to solve the overfitting and gradient vanishing (exploding) problems, which are issues with existing artificial neural networks. Overfitting is the decrease in the model's prediction accuracy for new data owing to the given training data, and the gradient vanishing (exploding) problem indicates a problem with artificial neural networks, whereas its weight slope converges to 0 or infinite as the training continues. The ReLU function alleviates these two problems by outputting 0 for below 0 and the existing value for 0 or higher. In addition, the differential calculation becomes simpler, and the training speed increases. The deep learning process can be divided into four stages:

1. Data acquisition.
2. Data preprocessing.
3. Modeling.
4. Model evaluation.

Data acquisition is the stage where data to be used for learning are collected from sensors and measurement devices. In this study, said data are the time-series data of voltage and current at each phase throughout the fault simulation. Data preprocessing is the stage where the collected data are preprocessed so that they are suitable for learning. Through the aforementioned wavelet transformation, the time-series data of voltage and current are converted to the data in the frequency domain and normalized between 0 and 1. Later, modeling uses the back propagation algorithm to tune the weights of the DNN based on the error rate obtained in the previous epoch.

$$L_{CE} = -\sum_{i=1}^{n} t_i \log(p_i) \tag{11}$$

Mean squared error (MSE) and cross-entropy error (CEE) are two loss functions that are widely used. MSE is sensitive to outliers by squaring the error, and errors less than 1 become smaller. Additionally, because squaring causes negative error values to become positive, it is difficult to determine whether they are underestimates or overestimates. In this study, CEE was used for the loss function, and with n number of classes, CEE is defined as shown in Equation (11). P is the output of the neural network, and T is the correct answer label. Additionally, in T, only the element of the index corresponding to the correct answer is 1, and the rest are 0 (one-hot encoding). Thus, Equation (11) actually calculates the natural logarithm of the estimate (Y when T is 1) when the answer is correct. Since T is 0 for all other answers, it does not affect the result even if it is operated with log. In

other words, the cross-entropy error determines the total value of the output when the answer is correct. The learning is performed in the direction where the difference between the estimated value in the learning process and the measured value is minimized. A loss function can be considered an index that expresses the performance of a neural network, and the higher the value from the loss function, the poorer the performance of the neural network. Therefore, a deep learning model aims to minimize the value of the loss function based on the CEE. Finally, the output model should be evaluated with new data that were not used for the training of said model to verify whether the learning was conducted well or whether there was overfitting. In the case of poor performance, problems should be identified in the previous stages and learning should be performed again after corrections.

3.3.2. Data Acquisition with PMU

PMU, which was developed due to the need for a synchronized measurement device after the major blackout in the USA in 1996, is often used to monitor the power transmission system over a wide area using the synchronization measurement function.

Table 2 shows the difference between RTU and PMU systems. The existing remote terminal unit (RTU) is installed with the line switchgear, which monitors the distribution line voltage and current in the normal stage via a distribution automation system (DAS) and transmits remote-control commands. In addition, it helps the fault detection and estimation of the location of the fault by detecting the fault current and voltage and transmitting the fault detection signal to the center in the case of a fault. However, the variability and intermittent characteristics of new renewable energy sources and power electronics devices require a change in the current periodic RMS-based monitoring method and the dependency on the central operation system's decision.

Table 2. Difference between RTU-based and PMU-based systems.

Type	RTU	PMU
Data measurement cycle (s)	2~10	1/10~1/60
Communication type	TCP	UDP
Observability	Normal	Dynamic/excessive

A PMU measures the magnitude, phase, and frequency of the voltage and current based on the universal time coordinates (UTC) received from the GPS. Each PMU grants a time tag independently through the GPS signal and the PMU's internal clock, which allows for the comparison at the same points at the time of each signal.

The most important one in the AI-based fault detection is that the measurement cycle should be short and accurate in order to block the circuit before the open conductor line makes contact with the ground. RMS-based monitoring by an RTU system cannot generate the input data required for open conductor fault detection.

3.3.3. Feature Extraction with Wavelet Transformation

Wavelet transformation is a method that converts the time domain to the frequency domain and constructs time information as a group of specific signals. These specific signals are called wavelets, and by expanding or contracting wavelets, it expresses the original waveform [26,27]. There have been attempts to use a frequency conversion method to detect ground faults or line-to-line short circuits more accurately and rapidly in a system [28–30]. However, the discrete Fourier transform (DFT) or short-time Fourier transform (STFT) used in the above studies could not deal with non-stationary characteristics. However, wavelet transformation uses a finite-duration basis function and is useful for transient signal analysis [31].

Wavelet transformation emerged to compensate for the shortcomings of the Fourier transformation. The output from the Fourier transformation does not have time information,

and thus, it is difficult to express the frequency that changes over time. STFT can solve this issue as it cuts the signal into small time units, performs a Fourier transformation, and feeds the result back to create one spectrogram. However, STFT has shortcomings. While it allows for a more accurate time zone in which a certain frequency is located as the time unit of the signal becomes smaller, if the cycle of the specific signal is longer than the time unit, it cannot sufficiently analyze the signal. Additionally, as the time unit of the signal becomes longer, the accurate time zone of the signal cannot be known. Owing to this tradeoff relationship between time and frequency, STFT is limited in not being able to improve both the frequency resolution and time unit at the same time.

Wavelet transform overcomes the above limitation by taking the time and frequency resolution separately through the scaling and shifting of the wavelet function. This is because the wavelet function used in the wavelet transformation is localized in time. As such, it can contain time information, and as shown in Figure 5a, different scales can be applied to specific time zones. A in Figure 5a requires temporal resolution so that the frequency resolution is lowered, while the opposite is the case for B. Figure 5b is the open conductor fault voltage signal measured in MATLAB. In Figure 5b, the upper graph is a time-series signal of voltage, and the lower figure expresses the wavelet-transformed signal as a scalogram. Figure 5a is a conceptual representation of the lower part of Figure 5b. The time-series signal of the voltage shows the addition of a harmonic signal after a fault has occurred. During the next three cycles, the harmonic signal gradually disappears. If the Fourier transform is used, it is difficult to express the transient phenomenon of the voltage signal because the time is unknown in the signal. However, the lower part of Figure 5b shows that the harmonic signal is fading. Since both time resolution and frequency resolution are high, it can be confirmed that the information of the signal is accurately expressed. There are various types of wavelet functions, and they should satisfy only the following two mathematical conditions so that they are useful to create a new type of function.

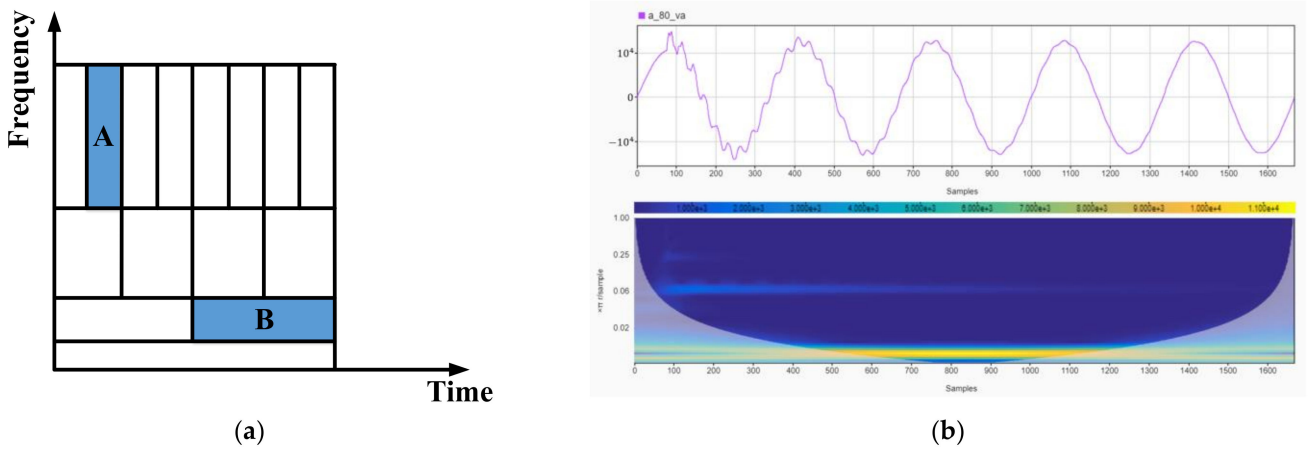

(**a**) (**b**)

Figure 5. Wavelet transform. (**a**) Wavelet transform concept diagram. (**b**) Open conductor fault voltage measured in a MATLAB simulation.

1. Finite energy:

$$E = \int_{-\infty}^{\infty} |\psi(t)|^2 dt < \infty \tag{12}$$

$$E = \int_{-\infty}^{\infty} |\psi(t)|^2 dt = E = \int_{-\infty}^{\infty} |\psi(t)|^2 df \tag{13}$$

2. Zero mean:

$$\int_{-\infty}^{\infty} \psi(t)dt = 0 \tag{14}$$

Finite energy means that a wavelet function is localized in time and frequency. This also signifies that a wavelet function can be integrated, and that the inner product of the wavelet and the signal exists at all times. Zero mean signifies that when the average of the wavelet is 0 and the frequency is 0, it is 0. This is the condition required for the integrable wavelet reverse calculation [32,33].

$$WT(a,b) = \frac{1}{|a|^{\frac{1}{2}}} \int_{-\infty}^{\infty} x(t)\overline{\psi}\left(\frac{t-b}{a}\right)dt \tag{15}$$

The wavelet function uses convolution to perform the calculation over the whole signal. The wavelet is expressed in Equation (15), where a and b show a scale factor and shift factor, respectively. A scale factor is a parameter that determines the size of a wavelet, and the smaller it is, the higher the frequency of the small wavelet produced. A shift factor is a factor for delaying the start of the wavelet, which shows that b is the center of the wavelet function. To match the wavelet to the characteristics from the signal, it is necessary to transform the wavelet. The order of the wavelet transformation is as follows:

1. Compare the wavelet at a small scale while transforming it from the start to the end of the signal. The degree of similarity between the signal and the wavelet is stored as the C coefficient.
2. Once the comparisons are completed to the end of the signal, the scale of the wavelet is expanded, and the process in step 1 is repeated.
3. The process is repeated up to the set scale.

From Equations (12)–(14), it can be determined that the basic wavelet function can have various types and is a finite function, where its integral is 0 and its amplitude converges to 0. As there are various types of basic wavelet functions, the result can differ by function even with an identical signal, and thus a suitable function should be selected. This study used a Gabor function as its basis. A complex Gabor function is expressed as a complex exponential, which can be expressed as the product of a Gaussian kernel and a complex sinusoid. This is shown in Equations (16) and (17):

$$g(x) = \frac{1}{\sqrt{2\pi\sigma}} e^{-\frac{x^2}{2\sigma^2}} (\cos(2\pi\omega_0 x) + i\sin(2\pi\omega_0 x)) \tag{16}$$

$$g(x) = \frac{1}{\sqrt{2\pi\sigma}} e^{-\frac{x^2}{2\sigma^2}} e^{-(2\pi\omega_0 x)} \tag{17}$$

Here, ω_0 is the center frequency, which is defined as the frequency where the filter produces the largest response, and σ is defined as the spread of the Gaussian window. If the real part of Equation (18) is Gabor sine and the imaginary part is Gabor cosine, the function can be expressed as follows:

$$g(x) = g_e(x) + ig_o(x) \tag{18}$$

$$g_e(x) = \frac{1}{\sqrt{2\pi\sigma}} e^{-\frac{x^2}{2\sigma^2}} \cos(2\pi\omega_0 x) \tag{19}$$

$$g_o(x) = \frac{1}{\sqrt{2\pi\sigma}} e^{-\frac{x^2}{2\sigma^2}} \sin(2\pi\omega_0 x) \tag{20}$$

EPRI research verified that *n* times the harmonic content of the fundamental frequency is measured at the neutral point in the case of an open conductor fault [15–19]. This means that the signal at fault is a trigonometrical function, such as the fundamental frequency. Therefore, this study used a Gabor function with finite-time wavelet functions, which is

similar to the trigonometrical function. Since the mother wavelet is finite, it is advantageous for expressing transient conditions such as line faults.

4. Implementation of Proposed Scheme for the Prevention of Wildfires

While it is ideal to use fault data in the actual system, they are difficult to obtain. When machine learning is performed with a small number of failure data, there is a risk of overfitting with signals that include noise. Therefore, in this study, data were acquired through simulation. Figure 6 is a simulation of an AC power system fault situation using MATLAB Simulink.

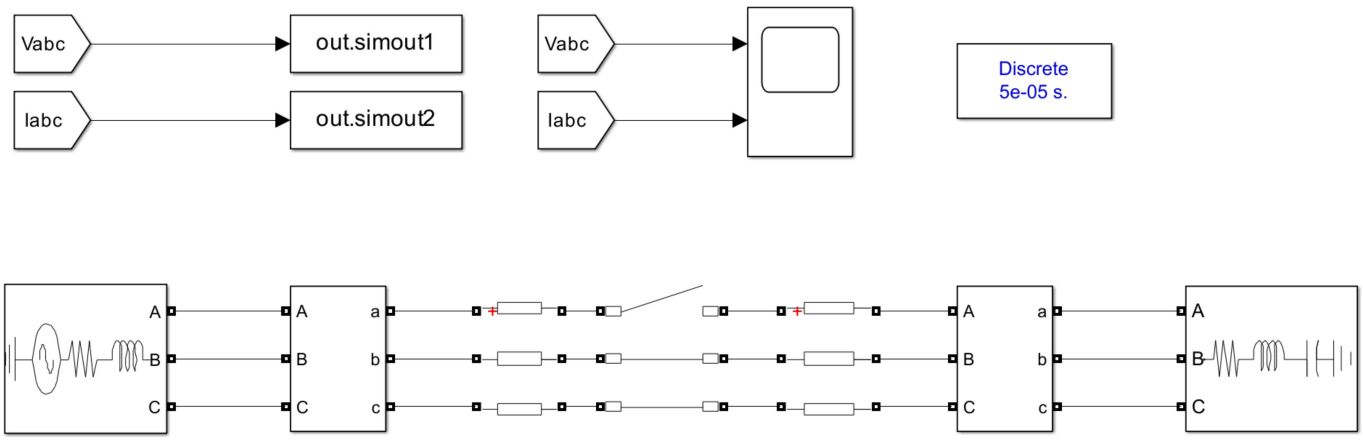

Figure 6. MATLAB open conductor fault simulation.

Figure 6 shows an open conductor fault simulation in MATLAB. The simulation was conducted using a three-phase electric power source, 100 km of overhead line, and the RLC load, the parameters of which are shown in Table 3. There are four fault locations that we can identify by dividing the 100 km line into five zones so that there is a 20 km difference between the locations, and the fault type was a single-phase open conductor fault on a, b, and c. Additionally, the phase was changed by 10° per fault so as to conduct a total of 432 fault simulations, as shown in Equation (21). The sample time of the simulation was 50 µs, and we measured the voltage and current from the sending end. Non-fault simulations were performed 36 times, totaling 468 simulations.

$$Fault\ point(4) \times Fault\ type(3) \times Phase(36) = Fault\ simulation\ times 432 \quad (21)$$

Table 3. Simulation parameters.

	Parameter	Val
Three-phase source	Phase–phase voltage (kV)	15.4
	Frequency (Hz)	60
	Source resistance (Ohms)	0.8929
	Source impedance (H)	0.0165
Three-phase series load	Nominal phase–phase voltage (kV)	15.4
	Nominal frequency (Hz)	60
	Active power (MW)	30
	Inductance reactive power (MVar)	3
	Capacitive reactive power (Var)	100
Distributed parameter line	Line length (km)	100
	Resistance per unit length (Ohms/km)	0.01273
	Inductance per unit length (mH/km)	0.3864
	Capacitance per unit length (nF/km)	0.9337
		4.1264
		12.74
		7.751

As is shown in Table 1, as a result of calculating the falling speed of the overhead line, the circuit breaker operation must be completed within 0.2198 s, i.e., 0.2 s after the open conductor fault was simulated, to collect time-series data before ground contact.

4.1. Open Conductor Fault Signal Analysis

In this study, both the fault detection time and accuracy are important. However, with a rapid fault detection time, the accuracy drops as there are insufficient input data; conversely, sufficient detection accuracy would require many data, and they are therefore in a tradeoff relationship. Thus, model training should be conducted by comparing the accuracy and time of the model based on the input data. However, before that, if the fault signal is analyzed and the number of cycles of meaningful data is confirmed by checking the trend of the fault signal for each class, it is possible to develop an efficient fault diagnosis algorithm because the required data limit is set.

Figure 7 shows the current comparison by fault location when phase A is open. The horizontal axis represents the number of samples, and the vertical axis represents the sample size. In Equations (1)–(9), the fault current due to open was regarded as zero. However, considering the line impedance between the measuring point and the fault point, the actual fault current is not zero because there is a load that corresponds to the line. Therefore, after the fault current decreases to zero due to a load drop, there is a difference in the magnitude and frequency of the fault current depending on the line impedance. In Figure 7, the blue signal (A 80 km Ia) has a higher current peak and a smaller frequency than the yellow signal (A 20 km Ia). For a blue signal with a longer line, more current flows because it is considered more loaded. In addition, when the electrical and mechanical forces are unequal, the frequency changes. When the load drops, the frequency tends to rise due to oversupply. Therefore, the yellow signal has a high frequency. Since the line impedance is maintained until the line touches the ground and impedance is added, the fault current data can be considered meaningful in all time domains.

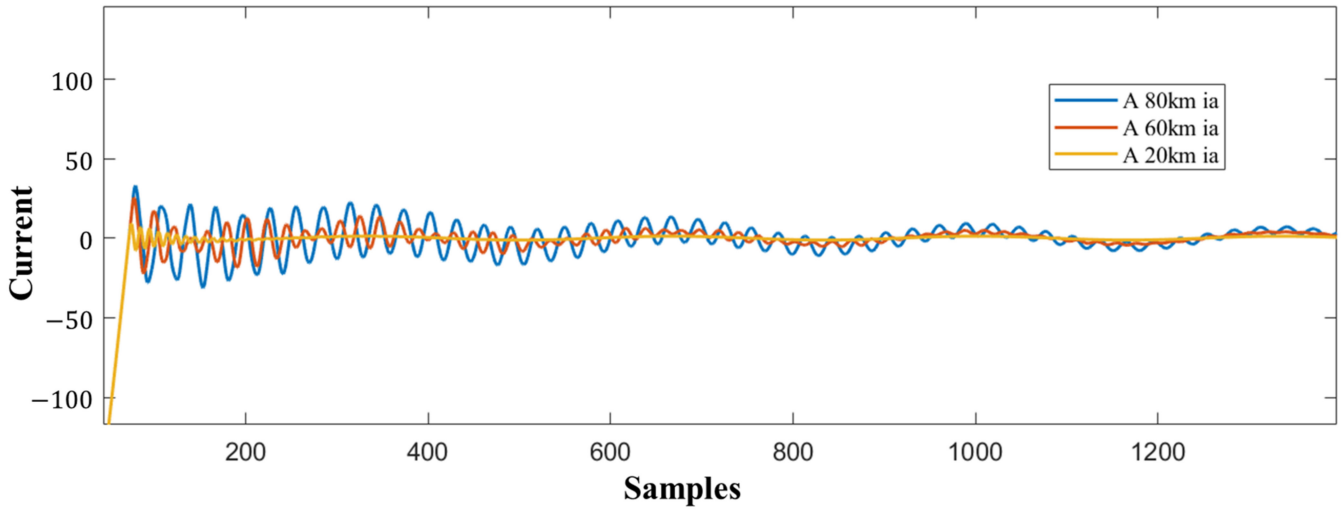

Figure 7. Fault current of phase A by distance.

Figure 8 shows the three-phase voltage by distance in the case of an A-phase open fault. Since a single-phase fault is an unsymmetrical fault, the voltage imbalance can be confirmed, as in Figure 9a,b. This means that fault/normal diagnosis is possible through voltage imbalance, but it is not helpful for fault location classification. There is almost no change in the overall size of the voltage waveform, which is the effect of the simulation on the three-phase constant voltage source. In practice, the bus voltage in the system is constantly controlled and will show the same pattern as in the simulation. According to Ohm's law, V = IZ, if the impedance is constant, the current is proportional to the voltage. As described above, because the impedance is constant before the line contacts the ground,

the harmonic component of the voltage is proportional to the frequency of the current in the case of an open fault. Therefore, the shorter and closer the line, the higher the frequency of the voltage harmonics.

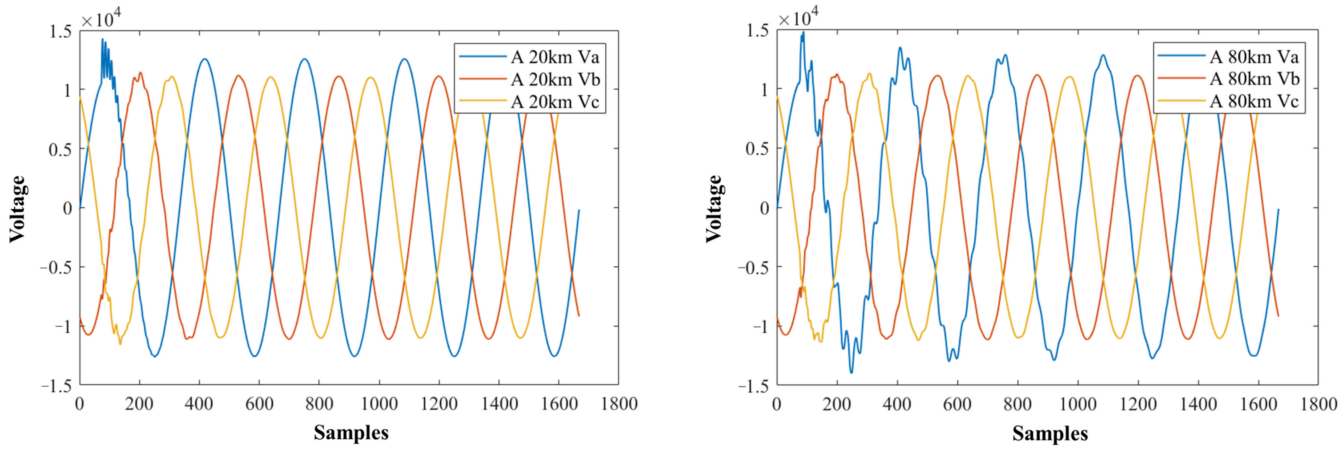

(**a**) (**b**)

Figure 8. Fault voltages by distance: (**a**) 20 km and (**b**) 80 km.

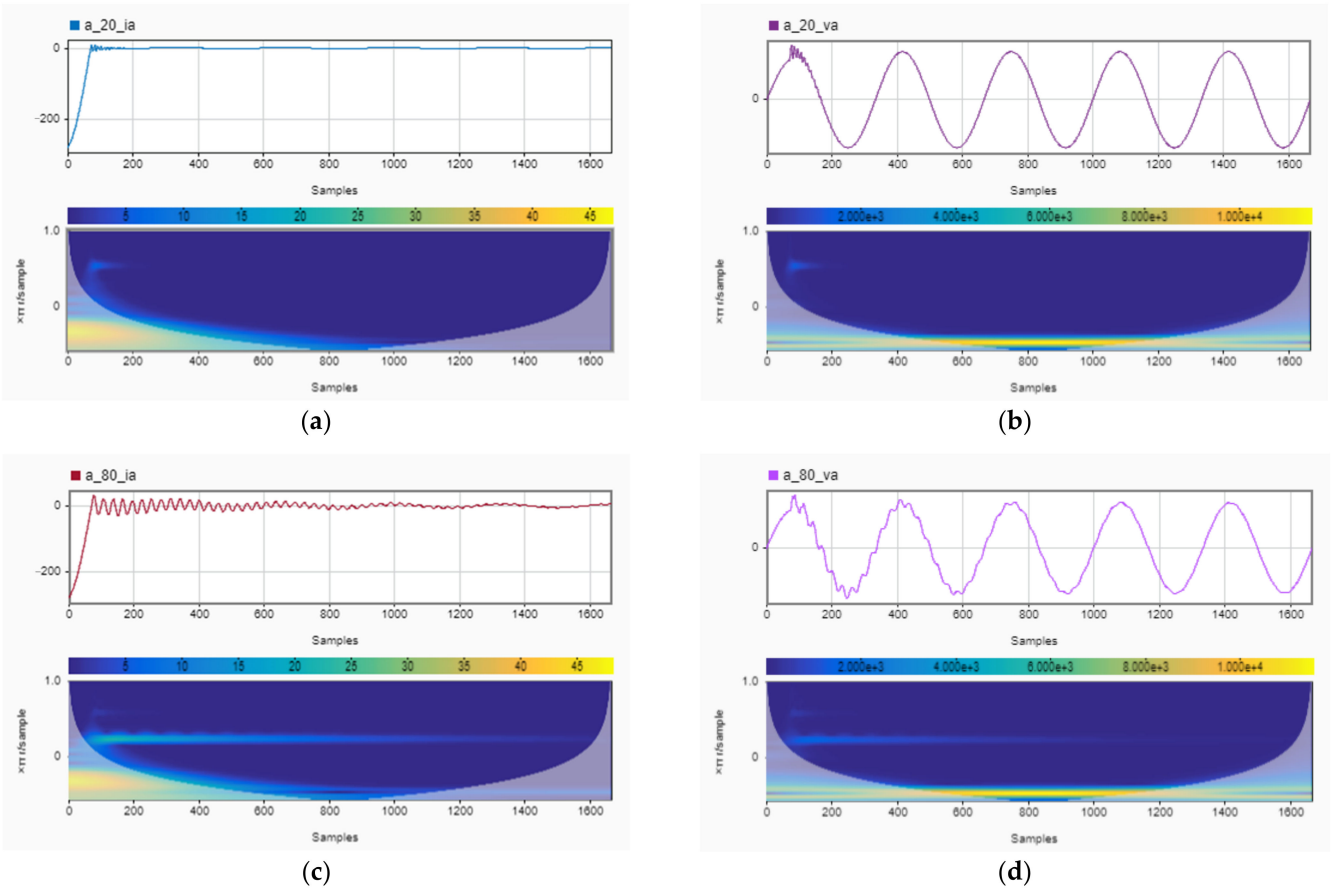

(**a**) (**b**)

(**c**) (**d**)

Figure 9. Phase A fault signal scalogram: (**a**) 20 km fault current, (**b**) 20 km fault voltage, (**c**) 80 km fault current, and (**d**) 80 km fault voltage.

Figure 9 shows the time and frequency domains of fault voltage and current. It takes 0.004 s for the fault current to converge to 0, and then a high-frequency signal is generated that corresponds to the line length (impedance). This affects the voltage signal,

and harmonic components proportional to the current frequency are added to the voltage signal. Figure 9a,b show the current and voltage at 20 km, and Figure 9c,d show them at 80 km. It can be seen that the scalograms of (a) and (b) are similar. Additionally, the tendencies of the frequency components of (c) and (d) are the same.

As a result of analyzing the disconnection fault signal, it is shown that the harmonic signal is commonly detected from the $\frac{1}{4}$ cycle (about 0.004 s), and after that it gradually disappears. Thus, it is determined that the input data at or over $\frac{1}{4}$ cycle would be the minimum condition.

Additionally, from Figure 9, it is determined that the trends become similar after three cycles as there is no new frequency component, except the amount of the harmonic wave content, confirming that the value of input data after three cycles is insignificant.

4.2. Input Data

As is shown in Figure 4, a three-phase voltage current is used as the input. Voltage and current time-series signals are expressed in the frequency domain. Additionally, it is flattened. Figure 10 is a mesh plot showing the time-series data of the phase A current in simulations performed 468 times.

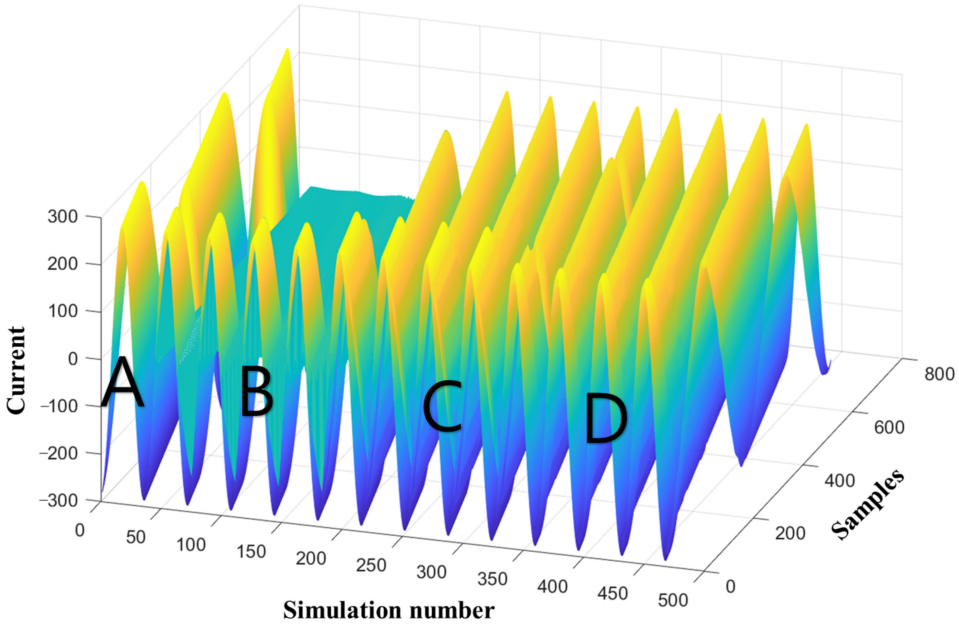

Figure 10. Phase A current by fault type.

Figure 11 shows flattened data, and these data include features of frequency components. A–D in Figures 10 and 11 are normal, phase A fault, phase B fault, and phase C fault data, respectively. A is simulation numbers 1~36, B is 37~180, C is 181~324, and D is 325~468. It is confirmed that each of the four classes has a different trend. However, diagnosing faults through the thresholds of each frequency is a difficult task. Therefore, artificial neural networks are applicable because they are specialized for solving classification problems.

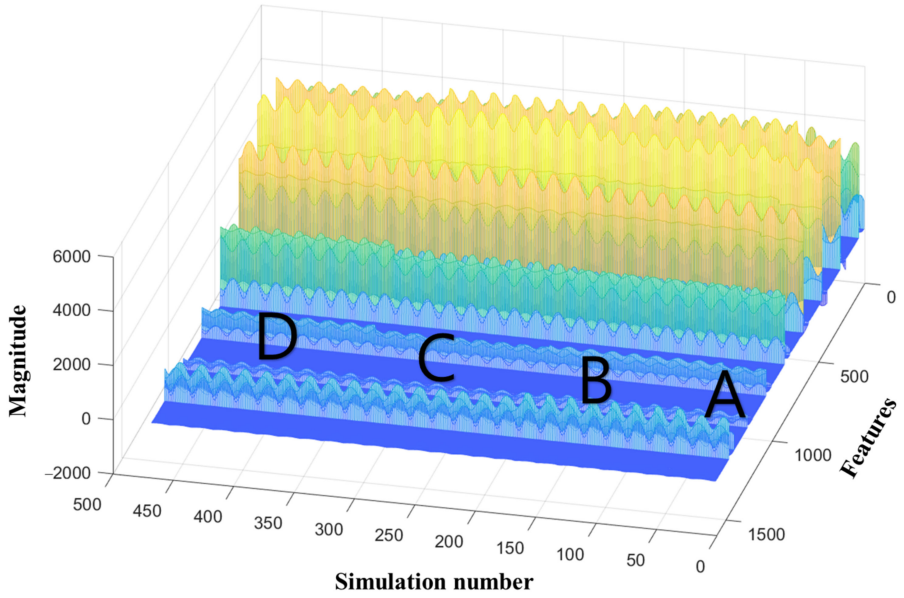

Figure 11. Input data-flattened frequency components by fault type.

4.3. Open Conductor Fault Location Classification Model

The training of the open conductor fault location identification model was performed so that the model could determine five classes: the class from the normal data, and four classes from the simulation data where the fault occurred at 20, 40, 60, and 80 km, respectively. Using 36 normal data and 432 fault data, the study trained the model with a total of 468 simulation data. A total of 70% of the data were used as training data, 15% as test data, and the remaining 15% as validation data.

Figures 12 and 13 are models trained with 1/4 cycles and 1/2 cycles as input data, respectively. It is confirmed that the model using the 1/4 cycle as an input did not learn properly due to insufficient input data. Figure 13 is the confusion matrix of the model using 1/2 cycles. The accuracy can be considered as high as 94.4%, but it is difficult to use because it can cause dangerous results when a fault is classified as normal.

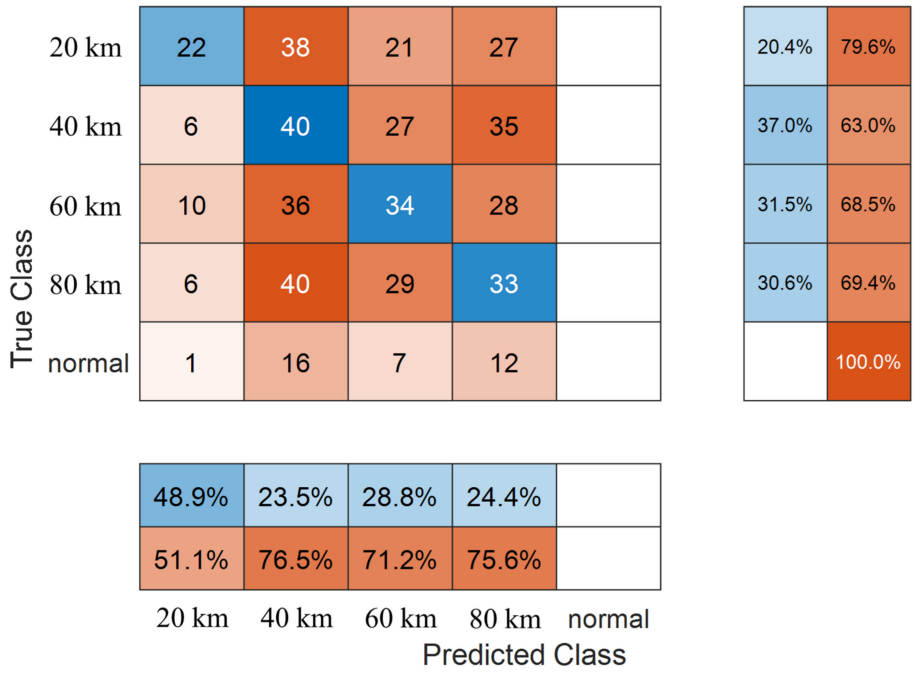

Figure 12. Confusion matrix of fault location classification model with 1/4 cycle data input.

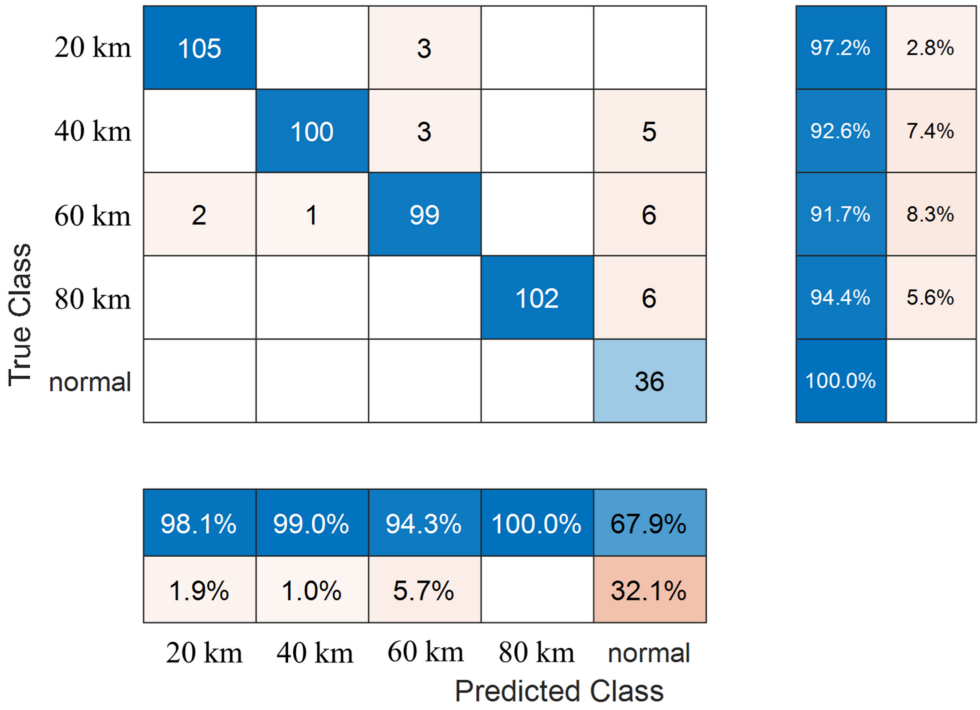

Figure 13. Confusion matrix of fault location classification model with 1/2 cycle data input.

Figure 14 shows the accuracy of the failure location classification model for each input cycle. In the disconnection fault signal analyzed above, if only the 1/4 cycle, which is the minimum data requirement, is used, the accuracy is very low. This is because learning was performed using only the transient signal converging to 0, not the high-frequency signal. Since it shows 100% accuracy after 1 cycle, it is most efficient to use 1 cycle as the input data to trip the circuit breaker before the line touches the ground.

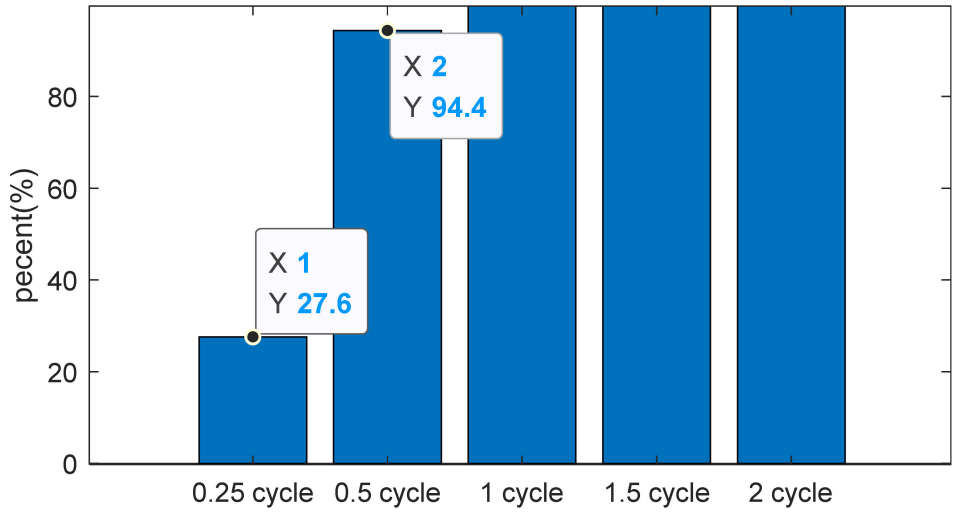

Figure 14. Model accuracy for open conductor fault location classification by input cycle.

Figure 15 is the CEE of the fault location classification algorithm according to the input cycle. The accuracy increases as the input data period increases. In the 1/4 cycle, the CEE of the test has a high value of 0.3404, but that of the 1/2 cycle is 0.0665 and of 1 cycle is 0.00000032098, which is close to zero.

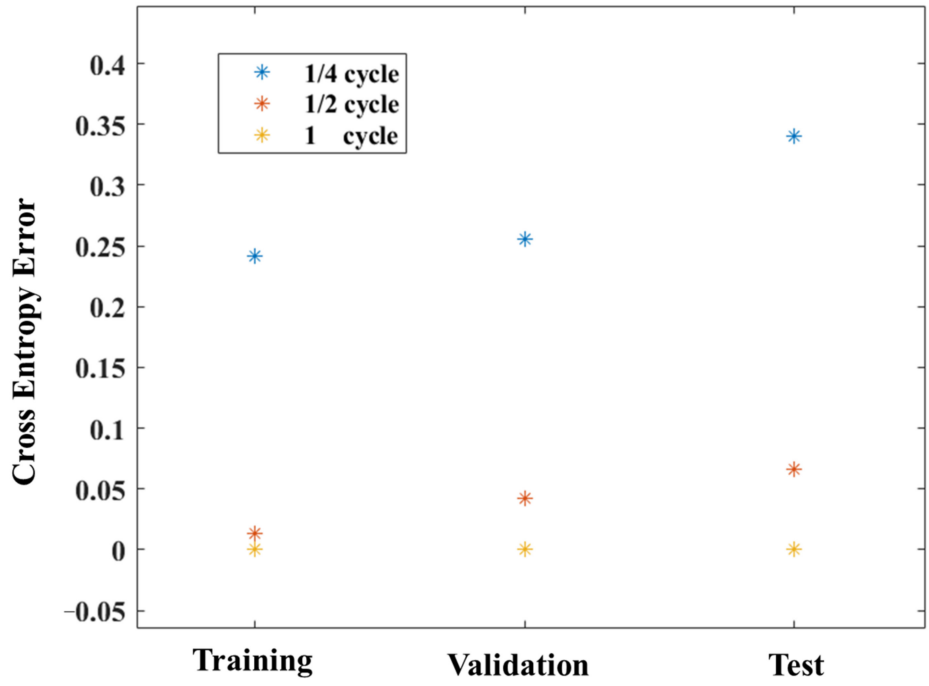

Figure 15. Fault location CEE by input cycle.

4.4. Open Conductor Fault Type Classification Model

An open conductor fault type classification model was also trained with the same dataset. The training rate also progressed to 70%, 15%, and 15%, and there were four classes. Figures 16 and 17 are the confusion matrices of the models that learned with 1/4 and 1/2 cycles as inputs, respectively.

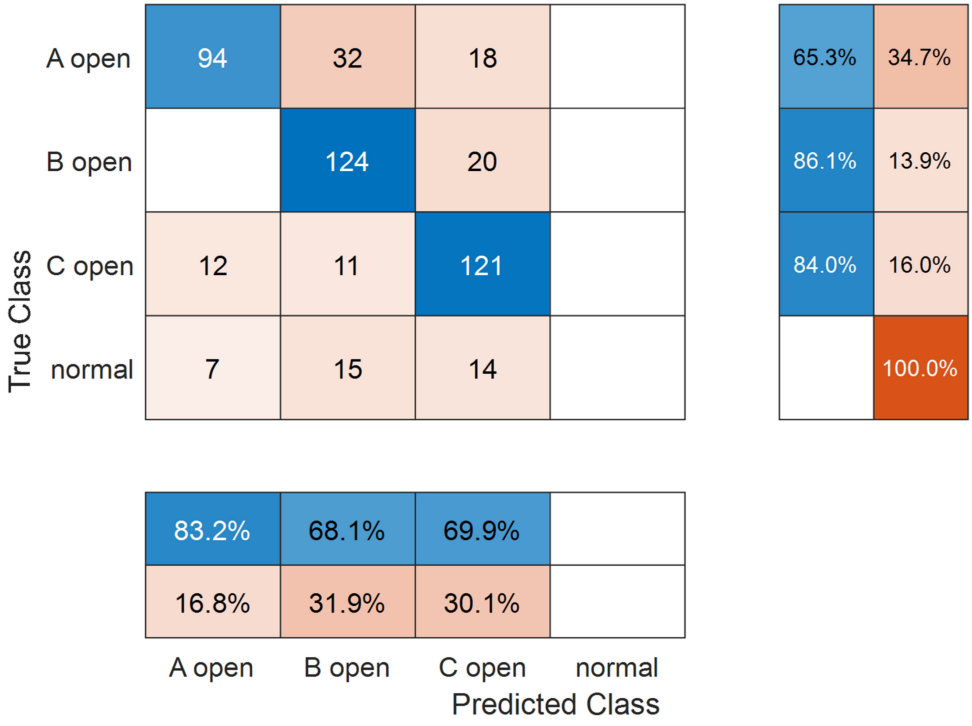

Figure 16. Confusion matrix of fault type classification model with 1/4 cycle data input.

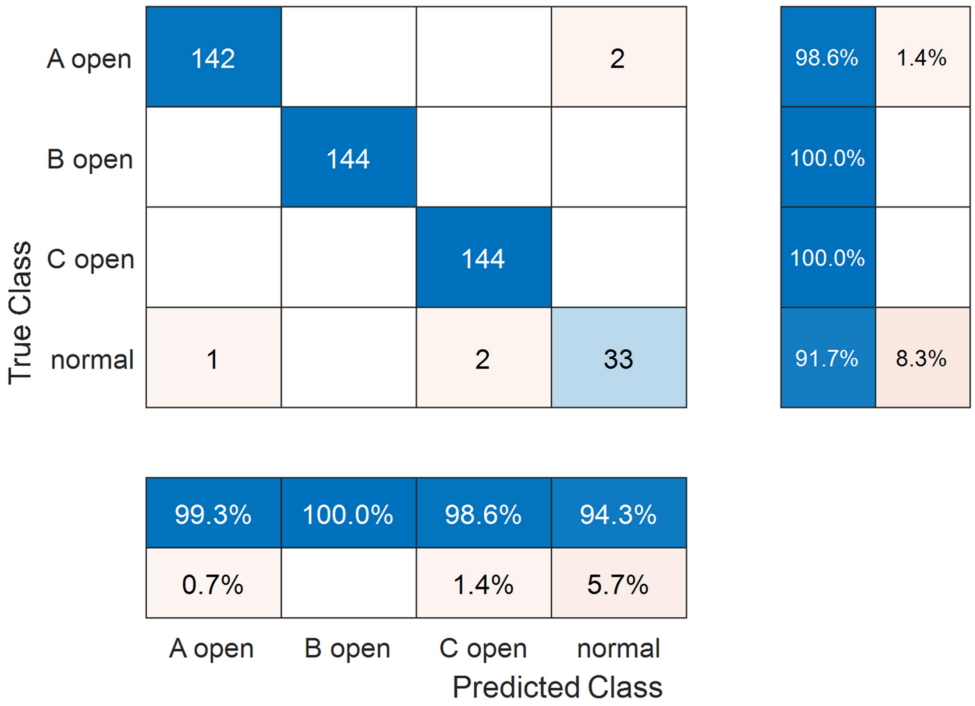

Figure 17. Confusion matrix of fault type classification model with 1/2 cycle data input.

In Figure 16, the fault type classification model shows higher accuracy than the fault location classification model. In Equations (1)–(9), it is assumed that the current of the faulty phase is zero. In addition, through open conductor fault analysis, it was confirmed that the current in the fault phase has a value close to zero. Therefore, since the fault phase converges to 0 after the 1/4 cycle, the classification difficulty is relatively low, and the accuracy is high.

Figure 17 shows 98.9% accuracy as a result of the failure type classification model using the 1/2 cycle. This also shows higher accuracy. In Figure 18, since the accuracy is 100% after one cycle of input data, it is easy to use one cycle of data. Using the 1/2 cycle as an input can also be considered, but 98.9% in a real-time monitoring system is not as high as expected. Even if the accuracy is 99.9%, the probability of obtaining the correct answer 1000 times in a row is 36.77%. Therefore, the optimal input for the open conductor fault classification model is one cycle.

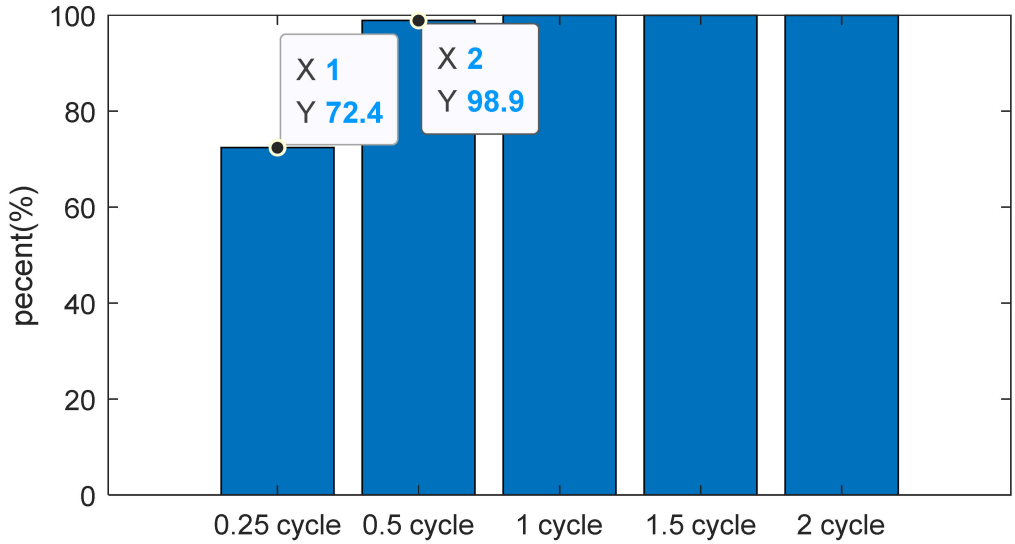

Figure 18. Model accuracy for open conductor fault type classification by input cycle.

Figure 19 shows the CEE of the fault type classification algorithm according to the input cycle. Similar to the fault location classification algorithm, the accuracy also increases as the input data cycle increases. With the 1/4 cycle, the CEE of the test is 0.2224; however, the CEE of the 1/2 cycle and 1 cycle are 0.0072 and 0.00000033744, respectively.

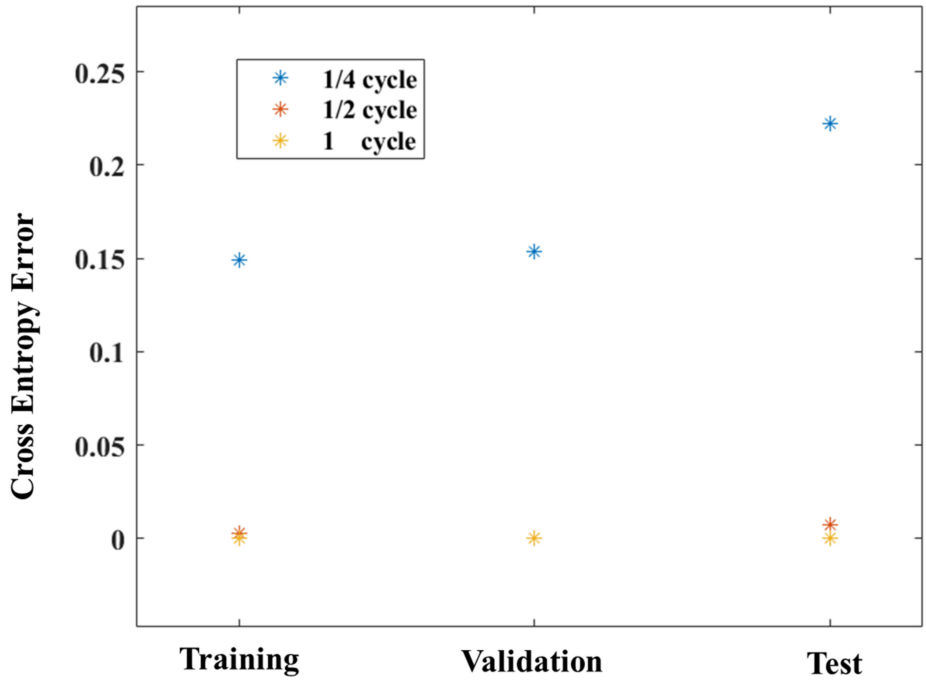

Figure 19. Fault type CEE.

4.5. Detection Time of Open Conductor Fault Classification Model

The total duration required for the circuit break can be calculated by summing the input data time (voltage, current, n cycle), the feature extraction (frequency conversion) time, the time for the classification of DNN, the communication time, and the circuit breaker operation (arc extinction) time. The time taken by the algorithm is processor-dependent, but if feature extraction takes 40–55 ms, the DNN's run time is 20–25 ms. Since the PMU can transmit data 30 times per second, the communication time is 34 ms and the circuit breaker operation time is 34~50 ms, so the total required time is calculated as shown in Table 4. The time it takes for feature extraction and DNN operation was based on a computer with an Intel(R) Core (TM) i7-10700 CPU @ 2.90 GHz processor. Since the CPU's GFLOPS is 461, faster open conductor fault detection is possible if a high-level FPGA is applied in the field. Xilinx Virtex-7 980XT FPGA offers 987 GFLOPS and can guarantee a sufficient circuit break time.

Table 4. Comparison of open conductor fault detection algorithm by number of input data cycles.

Input Data Cycle	1/4 Cycle	1/2 Cycle	1 Cycle
Request of input data	4.16 ms	8.34 ms	16.67 ms
Feature extraction (wavelet transform)		40~55 ms	
Communication		34 ms	
Determination by DNN		20~25 ms	
Circuit breaker arc extinction time		34~50 ms (2~3 cycle)	
Total required time	132.16~168.16 ms	136.34~172.34 ms	144.67~180.67 ms
Accuracy (type)	72.4%	98.9%	100%
Accuracy (location)	27.6%	94.4%	100%

5. Conclusions

Since overhead lines are exposed to the outdoors, faults may occur in deteriorated locations owing to weather conditions. There is a risk of fire for a short period owing to arcs caused by open conductor lines, and conventional fault detection methods can determine faults only after the line makes contact with the ground or tower arms. Therefore, in this study, an AI-based open conductor fault detection method for overhead lines was constructed that performs a circuit break before the overhead line makes contact with the ground in order to prevent fires. By simulating open conductor faults with MATLAB, 432 fault data were collected. The open conductor fault signal was analyzed in the time and frequency domains, and the minimum cycle requirements for the fault classification algorithm were derived. Additionally, the fall time of a 154 kV line was calculated while considering the span, height, and sag. We calculated the falling time of an open overhead line. In order to complete the fault detection, communication, and operation of the circuit breaker within this time, the study compared the accuracy with different numbers of input data cycles for fault diagnosis. While a short cycle may lead to a short fault detection time, the lack of input data leads to poor accuracy. After training the model while considering the accuracy and speed of the detection, the optimal input cycle was derived by comparing the models with each other. By calculating the fall time of a 154 kV line as the movement of a pendulum, it was shown that the circuit breaker needs to trip within 219.8 ms. When adding the input data time, feature extraction time, communication time, DNN operation time, and the circuit breaker's arc extinction time together, the total time to circuit breaking was 136.34–180.67 ms, and therefore, it appears that the proposed model can prevent fires owing to line arcs. The data used for learning and verification in this study were simulation data. Since it is more accurate to use real data for verification, additional research is needed to verify the algorithm in the future. In addition, fault diagnosis algorithms, including the one developed in this study, are aimed at real-time fault diagnosis. Even if an algorithm that diagnoses once per second has an accuracy of 99.9%, the probability of achieving correct diagnoses for 1000 consecutive seconds is only 36.7%. This necessitates further research.

Author Contributions: Conceptualization, T.P. and J.C.; methodology, B.A. and J.P.; software, T.K. and S.P.; validation, T.K. and S.P.; formal analysis, J.C.; writing—original draft preparation, J.C.; writing—review and editing, T.P. and J.C. All authors have read and agreed to the published version of the manuscript.

Funding: This work was supported by the National Research Foundation of Korea (NRF) grant funded by the Korean government (MSIT) (No. NRF-2022R1A2C1013445). This research was supported by Korea Electric Power Corporation (Grant number: R22XO02-20).

Data Availability Statement: Not applicable.

Conflicts of Interest: The authors declare no conflict of interest.

References

1. Paithankar, Y.; Bhide, S. *Fundamentals of Power System Protection*; PHI Learning Pvt. Ltd.: Delhi, India, 2004; pp. 23–25.
2. Blackburn, J.; Domin, T. *Protective Relaying*, 4th ed.; CRC Press: Hoboken, NJ, USA, 2014.
3. Bo, Z.Q.; Jiang, F.; Chen, Z.; Dong, X.Z.; Weller, G.; Redfern, M.A. Transient based protection for power transmission systems. In Proceedings of the 2000 IEEE Power Engineering Society Winter Meeting, Conference Proceedings (Cat. No.00CH37077). Singapore, 23–27 January 2000; Volume 3, pp. 1832–1837. [CrossRef]
4. Abdelmoumene, A.; Bentarzi, H. A review on protective relays' developments and trends. *J. Energy S. Afr.* **2014**, *25*, 91–95. [CrossRef]
5. Wai, D.C.T.; Yibin, X. A novel technique for high impedance fault identification. *IEEE Trans. Power Deliv.* **1998**, *13*, 738–744. [CrossRef]
6. Ayrton, H. *The Electric Arc*; Cambridge University Press: Cambridge, UK, 2012.
7. Ivan, P.; Eavis, P. California Utility Customers May Be on Hook for Billions in Wildfire Damage. *The New York Times*, 9 July 2018.
8. Choobineh, M.; Mohagheghi, S. Power grid vulnerability assessment against wildfires using probabilistic progression estimation model. In Proceedings of the 2016 IEEE Power and Energy Society General Meeting (PESGM), Boston, MA, USA, 17–21 July 2016; pp. 1–5. [CrossRef]

9. Li, L.; Redfern, M.A. A review of techniques to detect downed conductors in overhead distribution systems. In Proceedings of the 2001 Seventh International Conference on Developments in Power System Protection (IEE), Amsterdam, The Netherlands, 9–12 April 2001; pp. 169–172.
10. Ghaderi, A.; Ginn, H.L., III; Mohammadpour, H.A. High impedance fault detection: A review. *Electr. Power Syst. Res.* **2017**, *143*, 376–388. [CrossRef]
11. Dhawas, P.V.; Bedekar, P.P.; Nandankar, P.V. Advancement in Radial Power Distribution Network Using High impedance fault Relay. In Proceedings of the 2020 IEEE 17th India Council International Conference (INDICON), New Delhi, India, 10–13 December 2020; pp. 1–6. [CrossRef]
12. Yong, H.; Minyou, C.; Jinqian, Z. High impedance fault identification method of the distribution network based on discrete wavelet transformation. In Proceedings of the 2011 International Conference on Electrical and Control Engineering, Wuhan, China, 15–17 April 2011; pp. 2262–2265. [CrossRef]
13. Kundu Mondal, M.; Debnath, S. High Impedance Fault Classification in UPFC Compensated Double Circuit Transmission Lines using Differential Power Protection Scheme. In Proceedings of the 2018 IEEE Applied Signal Processing Conference (ASPCON), Kolkata, India, 7–9 December 2018; pp. 54–58. [CrossRef]
14. Saleh, S.M.; Ibrahim, D.K. Non-linear high impedance earth faults locator for series compensated transmission lines. In Proceedings of the 2017 Nineteenth International Middle East Power Systems Conference (MEPCON), Cairo, Egypt, 19–21 December 2017; pp. 108–113. [CrossRef]
15. IEEE Power and Energy Society. *Downed Power Lines: Why They Can't Always Be Detected*; Technical Report PES-TR2; Formerly TPPESDPL3; IEEE: Piscataway, NJ, USA, 1989.
16. Ohura, Y.; Matsuda, T.; Suzuki, M.; Yamaura, M.; Kurosawa, Y.; Yokoyama, T. Digital distance relay with improved characteristics against distorted transient waveforms. *IEEE Trans. Power Deliv.* **1989**, *4*, 2025–2031. [CrossRef]
17. Pongthavornsawad, A.; Rungseevijitprapa, W. Broken Conductor Detection for Overhead Line Distribution System. In Proceedings of the 2011 Asia-Pacific Power and Energy Engineering Conference, Wuhan, China, 25–28 March 2011; pp. 1–4. [CrossRef]
18. Jayamaha, D.K.J.S.; Madhushani, I.H.N.; Gamage, R.S.S.J.; Tennakoon, P.P.B.; Lucas, J.R.; Jayatunga, U. Open conductor fault detection. In Proceedings of the 2017 Moratuwa Engineering Research Conference (MERCon), Moratuwa, Sri Lanka, 29–31 May 2017; pp. 363–367. [CrossRef]
19. Al-Ghannam, S.H.; Khan, Y.; Ahmad, U.; Malik, N.H.; Al-Arainy, A.A.; Al-Shahrani, B.S. Development of open (Broken) conductor detection system for high resistivity areas. In Proceedings of the 2017 Saudi Arabia Smart Grid (SASG), Jeddah, Saudi Arabia, 12–14 December 2017; pp. 1–8. [CrossRef]
20. Johnson, W. *Nuclear Maintenance Application Center: Development and Analysis of an Open-Phase Detection Scheme for Various Configurations of Auxiliary Transformers*; EPRI: Palo Alto, CA, USA, 2013.
21. Johnson, W. *Interim Report: EPRI Open-Phase Detection Method*; EPRI: Palo Alto, CA, USA, 2014.
22. Aucoin, M.; Zeigler, J.; Russell, B.D. Feeder Protection and Monitoring System, Part II: Staged Fault Test Demonstration. *IEEE Trans. Power Appar. Syst.* **1985**, *PER-5*, 1455–1462. [CrossRef]
23. Benner, C.; Carswell, P.; Russell, B.D. Improved Algorithm for Detecting Arcing Faults Using Random Fault Behavior. *Electr. Power Syst. Res.* **1989**, *17*, 49–56. [CrossRef]
24. Westrom, A.C.; Meliopoulos, A.P.S.; Cokkinides, G.J.; Ayoub, A.H. Open conductor detector system. *IEEE Trans. Power Deliv.* **1992**, *7*, 1643–1651. [CrossRef]
25. Al-Ogaili, A.S.; Aris, I.; Othman, M.L.; Azis, N.B.; Isa, D.; Hoon, Y. New technique for decreasing of total harmonic distortion of three-phases bridge rectifier by using the method of harmonic injection. In Proceedings of the 2016 IEEE Conference on Systems, Process and Control (ICSPC), Melaka, Malaysia, 16–18 December 2016; pp. 248–253. [CrossRef]
26. Sharma, Y.K.; Vijay, M.R. Capacitor Banks and its Effect on Power System with High Harmonics Loads. In Proceedings of the 2018 3rd International Conference for Convergence in Technology (I2CT), Pune, India, 6–8 April 2018; pp. 1–6. [CrossRef]
27. Barr, R.A.; Gosbell, V.J. Power system harmonic voltage limits for the future. In Proceedings of the 2014 16th International Conference on Harmonics and Quality of Power (ICHQP), Bucharest, Romania, 25–28 May 2014; pp. 483–487. [CrossRef]
28. Wang, X.; Xu, W. A 3rd Harmonic Power Based Open Conductor Detection Scheme. *IEEE Trans. Power Deliv.* **2021**, *36*, 1041–1050. [CrossRef]
29. Wang, X.; Ding, T.; Xu, W. An Open Conductor Condition Monitoring Scheme Using Natural Voltage and Current Disturbances. *IEEE Trans. Power Deliv.* **2019**, *34*, 1193–1202. [CrossRef]
30. Gilany, M.; Al-Kandari, A.; Hassan, B. ANN based technique for enhancement of distance relay performance against open-conductor in HV transmission lines. In Proceedings of the 2010 The 2nd International Conference on Computer and Automation Engineering (ICCAE), Singapore, 26–28 February 2010; pp. 50–54. [CrossRef]
31. Rangade, A.N.; Sharma, R. ANN Based Open Conductor Fault Detector for Protection of Two Parallel Circuit Transmission Line. *Int. Res. J. Eng. Technol. (IRJET)* **2019**, *6*, 87–92.
32. Aker, E.; Othman, M.L.; Veerasamy, V.; Aris, I.b.; Wahab, N.I.A.; Hizam, H. Fault detection and classification of shunt compensated transmission line using discrete wavelet transform and naive bayes classifier. *Energies* **2020**, *13*, 243. [CrossRef]
33. Shahriar Rahman, F.; Sarker, Y.; Kumar Sarker, S.; Sheikh, M.R.I. Self attention convolutional neural network with time series imaging based feature extraction for transmission line fault detection and classification. *Electr. Power Syst. Res.* **2020**, *187*, 106437.

34. Jivitesh Nitin, C.; Kale, A.A.; Deore, S.R. Transmission Line Fault Detection Using Wavelet Transform & ANN Approach. In Proceedings of the 2022 IEEE Integrated STEM Education Conference (ISEC), Virtual, 26 March 2022.
35. Adly, A.R.; Abdel Aleem, S.H.E.; Algabalawy, M.A.; Jurado, F.; Ali, Z.M. A novel protection scheme for multi-terminal transmission lines based on wavelet transform. *Electr. Power Syst. Res.* **2020**, *183*, 106286. [CrossRef]
36. Fahim, S.R.; Sarker, S.K.; Muyeen, S.M.; Das, S.K.; Kamwa, I. A deep learning based intelligent approach in detection and classification of transmission line faults. *Int. J. Electr. Power Energy Syst.* **2021**, *133*, 107102. [CrossRef]
37. Belagoune, S.; Bali, N.; Bakdi, A.; Baadji, B.; Atif, K. Deep learning through LSTM classification and regression for transmission line fault detection, diagnosis and location in large-scale multi-machine power systems. *Measurement* **2021**, *177*, 109330. [CrossRef]
38. Nuthalapati, B.; Umesh, K.S. Detection of downed or Broken power line Fault not touching the ground. *J. Eur. Des Systèmes Autom.* **2018**, *51*, 309. [CrossRef]
39. Mabeta, S.J. Open Conductor Faults and Dynamic Analysis of a Power System. Master's Thesis, Institutt for Elkraftteknikk, Trondheim, Norway, 2012.
40. Kundur, P. Power system stability. In *Power System Stability and Control*; McGraw-Hill Education: New York, NY, USA, 2007.
41. Tziouvaras, D.A.; Altuve, H.J.; Calero, F. Protecting mutually coupled transmission lines: Challenges and solutions. In Proceedings of the 2014 67th Annual Conference for Protective Relay Engineers, College Station, TX, USA, 31 March–3 April 2014.
42. National Fire Protection Association, NESC. *National Electrical Safety Code*; IEEE: Picataway, NJ, USA, 2017.
43. Yesilyurt, B. Equations of Motion Formulation of a Pendulum Containing N-point Masses. *arXiv* **2019**, arXiv:1910.12610.
44. Oluwajobi, F.I. Effect of sag on transmission line. *J. Emerg. Trends Eng. Appl. Sci.* **2012**, *3*, 627–630.
45. Fortescue, C.L. Method of Symmetrical Co-Ordinates Applied to the Solution of Polyphase Networks. *Trans. Am. Inst. Electr. Eng.* **1918**, *37*, 1027–1140. [CrossRef]